


## Universality of $\mathbb{Z}_3$ parafermions via edge-mode interaction and quantum simulation of topological space evolution with Rydberg atoms

Asmae Benhemou <sup>1</sup>, Toonyawat Angkhanawin <sup>2</sup>, Charles S. Adams,<sup>2</sup> Dan E. Browne <sup>1</sup> and Jiannis K. Pachos<sup>3</sup>

<sup>1</sup>*Department of Physics and Astronomy, University College London, London WC1E 6BT, United Kingdom*

<sup>2</sup>*Joint Quantum Centre (Durham-Newcastle), Department of Physics, Durham University, South Road, Durham DH1 3LE, United Kingdom*

<sup>3</sup>*School of Physics and Astronomy, University of Leeds, Leeds LS2 9JT, United Kingdom*



(Received 25 January 2022; accepted 2 November 2022; published 1 May 2023)

Parafermions are  $\mathbb{Z}_n$  generalizations of Majorana quasiparticles, with fractional non-Abelian statistics. They can be used to encode topological qudits and perform Clifford operations by their braiding. Here we investigate the generation of quantum gates by allowing  $\mathbb{Z}_3$  parafermions to interact in order to achieve universality. In particular, we study the form of the nontopological gate that arises through direct short-range interaction of the parafermion edge modes in a  $\mathbb{Z}_3$  parafermion chain. We show that such an interaction gives rise to a dynamical phase gate on the encoded ground space, generating a non-Clifford gate which can be tuned to belong to even levels of the Clifford hierarchy. We illustrate how to access highly noncontextual states using this dynamical gate. Finally, we propose an experiment that simulates the braiding and dynamical evolutions of the  $\mathbb{Z}_3$  topological states with Rydberg atom technology.

DOI: [10.1103/PhysRevResearch.5.023076](https://doi.org/10.1103/PhysRevResearch.5.023076)

### I. INTRODUCTION

Fault-tolerant quantum computing schemes were shown to exist using error-correcting techniques [1–3] aimed at diminishing logical error rates by minimizing the error rate on individual gates. In this context, physical systems that provide access to a set of exact elementary gates are advantageous. Topological quantum computation was introduced as a way to provide a computational framework for fault-tolerant quantum computation by Kitaev, Freedman, and Preskill [4,5], which directly addresses the very low error rate requirement. The proposal is based on the use of anyons, i.e., localized two-dimensional many-body quantum systems that display exotic exchange statistics. While the braiding of Abelian anyons is characterized by an arbitrary phase factor, the statistics of non-Abelian anyon exchange are described by representations of the braid group. The non-Abelian character renders these objects useful for computation, which is carried out by creating pairs of anyons from the vacuum, inducing operations by adiabatically moving them around each other and fusing them, with the classical outcome defined by the resulting charge types and a very low estimated error rate. Quasiparticle modes emerging in condensed matter systems have been shown to carry (projective) non-Abelian statistics which can be identified with known anyon models. The most prominent example of such objects is Majorana zero modes (MZMs),

whose exchange is described by statistics of the Ising model [6,7], and which were found to appear in a two-dimensional electron gas in the fractional quantum Hall (FQH) regime [8], as one candidate for an experimental realization.

Majorana fermions constitute the  $\mathbb{Z}_2$  case of the more general  $\mathbb{Z}_d$  parafermion model. The latter can be used to encode qudits, and provides a wider set of braiding evolutions, making it a more computationally powerful and attractive counterpart [9]. Indeed, in contrast with Majorana sparse encoding where additional measurements are required [10], parafermions can provide a scalable entangling gate by braiding alone [11,12]. Much like MZMs, proposals to realize non-Abelian anyons typically consist of exploiting the edge states of FQH systems. In the following, we consider parafermionic zero-energy modes proposed to appear at the edges of suitably defined one-dimensional fractional topological superconductors [11,13], arising in Hamiltonians described by Ref. [9].

The braid group representation describing Ising and parafermionic statistics provides a reliable implementation of Clifford gates, but does not extend to a universal quantum gate set and can therefore be efficiently simulated classically [14,15]. Proposals exist to remedy this drawback for Majorana qubits, by allowing for additional noisy nontopological operations which take the form of direct short-range edge-mode interaction, i.e., a tunneling process. Such operations can give rise to the  $\pi/8$  rotation that together with Clifford operations constitutes a universal set [16,17]. Parafermions generalize the Majorana encoding to topological qudits. For prime  $d$ , Clifford unitaries complemented by any arbitrary non-Clifford gate are sufficient for universal quantum computing (UQC) [18]. Hence, the parafermion edge-mode (PEM) interaction is expected to provide a noisy non-Clifford gate to be made

Published by the American Physical Society under the terms of the [Creative Commons Attribution 4.0 International](https://creativecommons.org/licenses/by/4.0/) license. Further distribution of this work must maintain attribution to the author(s) and the published article's title, journal citation, and DOI.

fault-tolerant using magic-state distillation (MSD) protocols. Such schemes have been extensively studied in particular for qudits of prime  $d$ .

Recent research has focused on quantum simulation with Rydberg atoms due to their versatility [19]. They offer strong and controllable long-range interactions realized by selecting different Rydberg states and applying a wide range of optical fields [20]. With the development of experimental techniques improving the controllability of individual Rydberg atoms, such as optical tweezers, these systems represent an effective tool for simulating many-body physics of both coherent or dissipative, in- or out-of-equilibrium systems. This can be achieved by engineering the system Hamiltonian in order to simulate various spin systems and quantum phases of matter [21–23]. Lienhard *et al.* and Verresen *et al.* [24,25] also suggested that geometric phases and topological effects can be probed with Rydberg atom-based quantum simulations. Additionally, Rydberg systems provide a way of encoding a qutrit by driving the Rydberg atom around three levels, using microwave lasers as described in Refs. [26,27], which is of interest in the light of works such as Ref. [28].

In the following, we investigate which family of gates the interaction between the PEMs of a  $\mathbb{Z}_3$  parafermion chain gives rise to. Our main result concerns the adequacy of such gates for UQC with parafermions. We have chosen to focus on the three-dimensional qutrit space in this study since it has the benefit of prime dimension and computational tractability, though many of the features that we uncover are likely to be generic. Besides, we also suggest how to use a Rydberg atom to simulate topological evolution of the ground state of the parafermion chain Hamiltonian.

This paper is organized as follows. In Sec. II, we describe the  $\mathbb{Z}_3$  parafermion chain and its edge modes, then briefly describe computation with parafermions and the Clifford hierarchy. In Sec. III we investigate the parafermion edge-mode interaction and its action on the ground state space. In Sec. IV we show that the addition of the dynamical gate available using the PEM interaction to the Clifford group, accessible through braiding operations, generates a gate set dense in  $SU(3)$ . In Sec. V, we discuss a potential physical implementation using a four-Rydberg-level atomic system interacting with four microwave lasers, in order to simulate the direct parafermion interaction and two-parafermion braiding. Finally, our results are discussed in Sec. VI.

## II. BACKGROUND

### A. The parafermion chain

In the following, we will consider a chain of  $\mathbb{Z}_3$  parafermions. In Ref. [9], Fendley introduced a variation of the Kitaev chain expressed in terms of parafermion operators, whose Hamiltonian takes the general form

$$H = - \sum_{j=1}^{L-1} J_j (\psi_j^\dagger \chi_{j+1} \alpha \bar{\omega} + \text{H.c.}) - \sum_{j=1}^L f_j (\chi_j^\dagger \psi_j \hat{\alpha} \bar{\omega} + \text{H.c.}), \quad (1)$$

where  $L$  is the length of the chain, and at each site  $j$  lie two parafermions  $\chi_j$  and  $\psi_j$ . The  $\omega = e^{\frac{2\pi i}{3}}$  factors ensure Hermiticity, and the couplings  $f_j$  and  $J_j$  are real and non-negative.

The above Hamiltonian can be rewritten in terms of the chiral clock model, by reexpressing the parafermion operators as

$$\chi_j = \left( \prod_{k=1}^{j-1} \tau_k \right) \sigma_j \text{ and } \psi_j = \omega \left( \prod_{k=1}^{j-1} \tau_k \right) \sigma_j \tau_j, \quad (2)$$

where  $\sigma$  and  $\tau$  generalize the usual Pauli  $\sigma^z$  and  $\sigma^x$  matrices to a three-dimensional space. These respectively characterize the flip and shift Hamiltonian terms in Eq. (1). For  $j < k$ , these operators follow the commutation relations

$$\chi_j \psi_j = \omega \psi_j \chi_j,$$

$$\chi_j \chi_k = \omega \chi_k \chi_j, \quad \psi_j \psi_k = \omega \psi_k \psi_j, \quad \chi_j \psi_k = \omega \psi_k \chi_j, \quad (3)$$

and one can verify that  $\chi_j^3 = \psi_j^3 = 1$  while each operator individually squares to its Hermitian conjugate. The three physical parameters of significance are the relative strengths of couplings in Eq. (1), and two angles  $\phi, \hat{\phi}$  which determine the parameters  $\alpha$  and  $\hat{\alpha}$ . In the following, we consider the symmetric case of  $\alpha = \hat{\alpha} = e^{-i\frac{\pi}{6}}$ , which lies at the midsection between the ferromagnetic and antiferromagnetic phases of the model in order to ensure chiral interactions and robust edge modes. Recent investigations of the parameter space of the system using DMRG tools offer detailed insight into the phases of this model [29,30].

### B. Parafermion edge modes

When both time-reversal and spatial-parity symmetries are broken, parafermion zero-energy modes can emerge in the parafermion chain, localized at its edges. These are characteristic of topological order, and described by the left and right edge-mode operators  $\Psi_L$  and  $\Psi_R$ , which obey the relations

$$[H, \Psi_L] = [H, \Psi_R] = 0, \quad \omega^P \Psi = \omega \Psi \omega^P, \quad (4)$$

where  $\omega^P = \prod_{j=1}^L \tau_j^\dagger$  is the  $\mathbb{Z}_3$  symmetry generator. These properties respectively describe that these are zero-energy modes, which map between  $\mathbb{Z}_3$  parity sectors, giving rise to the threefold degeneracy of the energy spectrum of  $H$ . From Eq. (1) it is clear that exact PEMs exist when  $f_i = 0 \forall i$  such that  $[H, \chi_1]_{f_i=0} = [H, \psi_L]_{f_i=0} = 0$  for a chain of length  $L$ .

Since the system exhibits an energy gap, one expects its PEMs to remain approximate zero modes for small enough  $f/J$ , with their support on the bulk of the chain exponentially suppressed in their distance to the bulk parafermions, as shown in Fig. 1(b). The left edge-mode operator of a chiral parafermion was constructed in Ref. [9] up to order  $f/J$  (where the couplings were taken to be uniform across the chain) using an iterative procedure, and takes the form

$$\Psi_L = \chi_1 - 2if e^{-i\hat{\phi}} X + 2if e^{i\hat{\phi}} \chi_1^\dagger Y + \dots, \quad (5)$$

where

$$X = \frac{1}{4J \sin(3\phi)} (\psi_1 + e^{2i\phi} \chi_2 + e^{-2i\phi} \omega \psi_1^\dagger \chi_2^\dagger) \quad (6)$$

and  $Y = -X^\dagger$ . It is straightforward to show that the right edge mode can be derived in a similar fashion. This procedure can be iterated, with the dimensionless expansion parameter  $f/[2J \sin(3\hat{\phi})]$ , but does not work at the approach of the

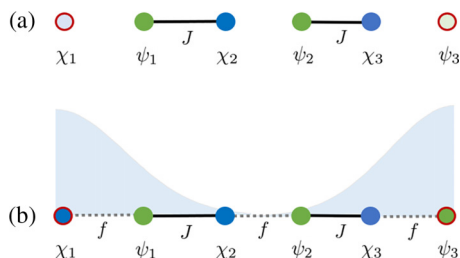


FIG. 1. Schematic of the localized (a) and delocalized (b) edge modes, such that the latter are described by extended operators as introduced in Eq. (5), where the  $\chi_i$  and  $\psi_i$  operators represent left and right parafermions occupying each site of the chain, as per Eq. (1). The shaded curves indicate their support on the bulk parafermions.

parity-invariant ferromagnetic and antiferromagnetic points. One can see that the symmetric points  $\phi = \frac{\pi}{6} \pmod{\frac{\pi}{3}}$  are the most robust for the existence of edge modes. We note that such edge modes have a strong character, necessary for such an analysis to hold [31].

### C. Computing with parafermions

Regardless of the underlying physical system which gives rise to parafermionic excitations, computation relies on the ability to adiabatically braid and fuse parafermions and distinguish between their fusion outcomes. Combining these capabilities realizes a set of exact unitary operators and measurements. In Ref. [12], Hutter and Loss derived the braiding operators acting on a logical qudit encoded using four  $\mathbb{Z}_n$  parafermions. In the qutrit case, one can write the most general unitary representation of such gates as

$$U_i = \frac{1}{\sqrt{3}} \sum_{m \in \mathbb{Z}_3} c_m (\Lambda_i)^m, \tag{7}$$

where  $\Lambda_i = \omega p_i p_{i+1}^\dagger$  are local parity operators for parafermions  $p_i$  and  $p_{i+1}$ , and  $c_m$  are coefficients derived by satisfying far commutativity and the Yang-Baxter equation [32]. The parity operators can be identified with  $\Lambda_{2i-1} = X_i^\dagger$  and  $\Lambda_{2i} = Z_i Z_{i+1}^\dagger$ , which admit the same spectrum as that of the generalized qutrit Pauli operators, namely  $\{1, \omega, \bar{\omega}\}$ . Hence, an eigenbasis  $\{|0\rangle, |1\rangle, |2\rangle\}$  can be defined for each parity operator such that  $\Lambda_i |m\rangle_i = \omega^m |m\rangle_i$ , for  $m \in \mathbb{Z}_3$ . These states form a basis of the fusion space of the pair of parafermions  $p_i$  and  $p_{i+1}$ . More generally, a three-dimensional Hilbert space is associated with each pair of parafermions. A qutrit can also be encoded into the fusion space of four parafermions  $\{p_1, p_2, p_3, p_4\}$ . The corresponding Hilbert space can be restricted under a global parity constraint  $\Lambda_1 \Lambda_3 = 1$ . The group of unitaries generated by  $U_1, U_2$ , and  $U_3$  as defined in Eq. (7) acts on this computational subspace, spanned by the states  $\{|0\rangle_1 |3\rangle_3, |1\rangle_1 |2\rangle_3, |2\rangle_1 |1\rangle_3\}$ . The authors showed that the braids  $U_1$  and  $U_1 U_2 U_1$  (up to global phases) respectively act on the logical space following

$$X \rightarrow XZ^\dagger, \quad Z \rightarrow Z \quad \text{and} \quad X \rightarrow Z, \quad Z \rightarrow X^\dagger.$$

These gates were proven to be necessary and sufficient to generate the single-qutrit Clifford group in Ref. [33]. In Fig. 2(a)

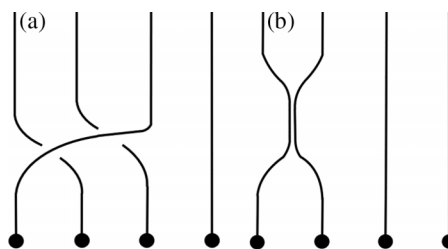


FIG. 2. Schematic of single-qutrit gates on a logical qutrit encoded in four parafermions denoted by the black dots. Their world lines are depicted as time flows upward. Panel (a) represents a topological  $S$  gate produced by parafermion braiding [12]. In panel (b) the closing distance between the world lines of the first two parafermions represents the nontopological dynamical gate accessible by parafermion edge-mode interaction.

we show the  $U_1 U_2 U_1$  braid which realizes the topological  $S$  gate. However, Clifford unitaries alone do not allow for universal quantum computing. In our study, we consider a similar approach to that in Ref. [17], namely allowing the parafermion modes to interact by bringing them close together so as to generate a dynamical non-Clifford unitary on the logical space.

### D. Clifford hierarchy

The theory behind quantum error correction and fault-tolerant computation relies upon access to gates from different levels of the Clifford hierarchy, defined by Gottesman and Chuang in Ref. [34] as

$$\mathcal{C}^{(k+1)} := \{U | U P U^\dagger \in \mathcal{C}^{(k)}, \forall P \in \mathcal{P}_n\}, \tag{8}$$

where  $\mathcal{P}_n := \mathcal{P}^{\otimes n}$  in the  $n$ -qudit Pauli group, generated by the  $\tau$  and  $\sigma$  matrices introduced in Eq. (2), and  $k$  indicates the level in the hierarchy [34]. With this definition, we can identify the Pauli and Clifford groups respectively as  $\mathcal{C}^{(1)}$  and  $\mathcal{C}^{(2)}$ . Higher levels are of interest for any  $d$ -dimensional qudit system in order to achieve universality, and in particular any gate from the third level  $\mathcal{C}^{(3)}$  supplementing the Clifford group generates a universal gate set. In the  $d = 2$  case, the  $T$  gate (i.e.,  $\pi/8$ -phase gate) plays a special role as a natural choice [35]. While in general for  $k \geq 3$  the gate sets in the Clifford hierarchy do not form a group, the subset of diagonal operators  $\mathcal{C}_d^{(k)} \subset \mathcal{C}^{(k)}$  does, making investigations for a  $T$ -gate qudit analog tractable as shown in Refs. [36–38]. In particular, Cui *et al.* showed that a diagonal gate  $U$  in any level of the Clifford hierarchy for qudits of dimension  $d$  can be written as

$$U = \sum_{j \in \mathbb{Z}_d} \exp\left(2\pi i \sum_m \delta_m(j)/d^m\right) |j\rangle \langle j|, \tag{9}$$

where  $\delta_m(j)$  is a polynomial over  $\mathbb{Z}_d^m$ , and the level of the Clifford hierarchy containing  $U$  is given by the degree of  $\delta_m(j)$  with the largest  $m$  [38]. In the following, this definition is used to characterize the unitary operator we obtain from parafermion edge-mode interaction.

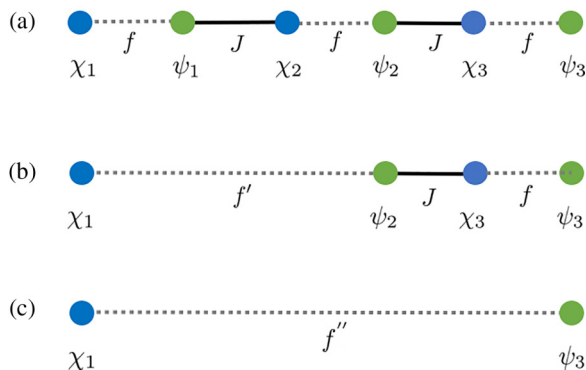


FIG. 3. Schematic of a three-site parafermion chain with weak  $f$  and strong  $J$  couplings defined as per Eq. (1), where the  $\chi_i$  and  $\psi_i$  represent the left and right parafermion operators at each site of the chain (a). The chains in (b) and (c) represent the decimation of the terms connecting parafermions in the bulk upon applying the RG method, with a final weaker effective coupling  $f''$ .

### III. A DYNAMICAL GATE FROM PARAFERMION INTERACTION

The main object of this section is to understand how parafermion edge modes interact when the  $f_i$  couplings in Eq. (1) are nonzero. This interaction ensures that one can induce a tunneling process by transporting such PEMs within a sufficient distance of each other, running the interaction for a desired time interval and returning the anyons to their initial positions, whereby a dynamical gate is applied on a qutrit encoded in the degenerate ground subspace of the system [10,17].

#### A. Decimation of the highest-energy term

The strongly interacting nature of parafermion systems makes their analytical study challenging, particularly the computation of their spectrum. A general approach is to use efficient DMRG techniques for numerical studies. In the following we use the real-space renormalization group method applied to the transverse-field Ising model by Fisher in Ref. [39]. This approach requires decimating the highest-energy term in the Hamiltonian and replacing it with effective longer-range interactions. Specifically, in the case of the Ising chain this prescribes decimating a spin if the stronger interaction is a field  $f_i$ , or forming a ferromagnetic cluster if it is a bond  $J_i$ . We extend this scope to a parafermion chain where the  $f_i$  on-site couplings are weak, such that the largest energy is the bond between chain sites as shown in Fig. 3(a) for a three-site chain. This process freezes the clock states at neighboring sites together in a ferromagnetic cluster with an effective field  $f' = \frac{f_i f_{i+1}}{2J_{i,i+1}}$ . This coupling is weaker than the individual  $f_i$  and  $f_{i+1}$  since the new interaction is a next-to-nearest-neighbor one, which decimates the interaction between sites  $i$  and  $(i+1)$  (i.e., a parafermion pair). This process is illustrated in Figs. 3(a)–3(c). Hence, the form of the Hamiltonian remains the same, apart from an overall constant shift in the spectrum, that can be neglected.

#### B. Effective Hamiltonian from PEM interaction

We first consider a two-site  $\mathbb{Z}_3$ -parafermion chain with a Hamiltonian  $H_2$  describing the two-site version of Fig. 3(a), such that  $H_2 = F_2 + V_2$  where

$$F_2 = -\frac{2}{\sqrt{3}} e^{-i\phi} \bar{\omega} (J_1 \psi_1^\dagger \chi_2) + \text{H.c.},$$

$$V_2 = -\frac{2}{\sqrt{3}} e^{-i\hat{\phi}} \bar{\omega} (f_1 \chi_1^\dagger \psi_1 + f_2 \chi_2^\dagger \psi_2) + \text{H.c.}, \quad (10)$$

and we set the phase parameters to  $\phi = \hat{\phi} = \frac{\pi}{6}$ . To define the Hamiltonian we chose the representation

$$\sigma = \begin{pmatrix} 1 & 0 & 0 \\ 0 & \omega & 0 \\ 0 & 0 & \omega^2 \end{pmatrix} \quad \text{and} \quad \tau = \begin{pmatrix} 0 & 0 & 1 \\ 1 & 0 & 0 \\ 0 & 1 & 0 \end{pmatrix}, \quad (11)$$

to express the parafermion operators in Eq. (2). The eigenspectrum of  $F_2$  is threefold degenerate, with eigenvalues  $\{-2J_1, 0, 2J_1\}$  and three degenerate ground states  $\{|e_0\rangle, |e_1\rangle, |e_2\rangle\}$ . When  $f_1$  and  $f_2$  are nonzero, the edge modes of the parafermion chain are no longer exactly localized, as described by Eq. (5). A perturbative treatment of the effect of  $F_2$  on the ground-state manifold, in terms of  $f_1/J_1$  and  $f_2/J_1$ , produces the effective coupling induced by an interaction between the edge parafermions  $\chi_1$  and  $\psi_2$  up to arbitrary order. The first-order perturbation vanishes for our system, while the second-order terms contribute to an effective Hamiltonian given by

$$H_2^{(2)} = -\frac{f_1^2 + f_2^2}{J_1} + \frac{f_1 f_2}{J_1} (\omega \chi_1 \psi_2^\dagger + \bar{\omega} \psi_2 \chi_1^\dagger), \quad (12)$$

where we can see that the first term is a global energy shift which we neglect, and the second term characterizes the interaction of the parafermion zero modes, which happens with a coupling  $f' = \frac{f_1 f_2}{J_1}$ , and acts on the ground-energy subspace with the following Hamiltonian,

$$H_2^{(2)} = \begin{pmatrix} 0 & \omega & \bar{\omega} \\ \bar{\omega} & 0 & \omega \\ \omega & \bar{\omega} & 0 \end{pmatrix}. \quad (13)$$

Following the prescription described in Sec. III A, the form of the second term in Eq. (12) indicates that the decimation of the parafermion pair  $(\psi_1, \chi_2)$  induces an  $f'$  interaction between the edge parafermions. This result is similar to the Majorana case explicitly shown in Ref. [40] where the coupling between Majorana zero modes takes an similar form for  $L = 2$ . We iterate the above decimation procedure for a chain of arbitrary length  $L$  by decimating bonds from left to right to derive the interaction between the edge modes of a chain of arbitrary size, as shown in Fig. 3. We find that the effective Hamiltonian up to second order in the energy perturbation is given by

$$H_L^{(2)} = -\frac{1}{J_{L-1}} \left( \frac{\prod_{i=1}^{L-1} f_i^2}{\prod_{i=1}^{L-2} J_i^2} + f_L^2 \right) + \frac{\prod_{i=1}^L f_i}{\prod_{i=1}^{L-1} J_i} (\omega \chi_1 \psi_L^\dagger + \bar{\omega} \psi_L \chi_1^\dagger). \quad (14)$$

The PEM interaction term remains exactly  $H_2^{(2)}$  in Eq. (13), and has an eigenspectrum of  $\{E_0 = 2A, E_1 = -A, E_2 = -A\}$  which now discriminates between the basis states up to a global  $\mathbb{Z}_3$  rotation, where the energy scale is given by

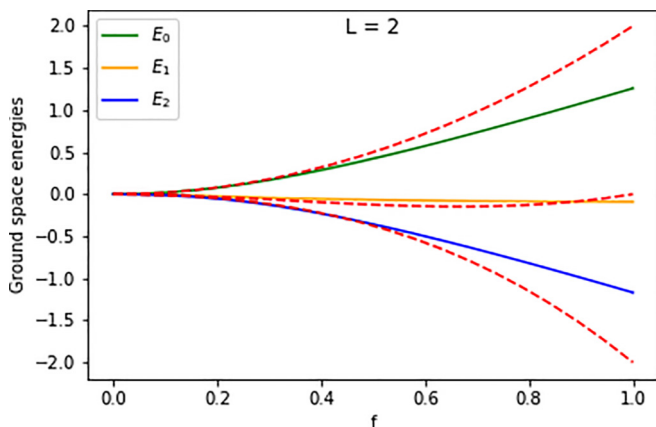


FIG. 4. Three lowest-energy eigenvalues for  $H_2$  with  $J_i = 1 \forall i$  and varying  $f$ . The numerical values are indicated by the continuous lines. The perturbative approximations up to third order are indicated with red dotted lines, which are in agreement with the exact results for a wide range of  $f$  values.

$A = \prod_{i=1}^L f_i / \prod_{i=1}^{L-1} J_i$ . The exact eigenvalues of the three lowest-energy states of  $H_2$  (for numerical convenience) are numerically plotted in Fig. 4 for  $f_i = f \forall i$  and  $J_i = 1 \forall i$ , where the global energy shift was deducted. The degeneracy is lifted by the splitting of the eigenstates when  $f \neq 0$ . The energy shifts obtained using the decimation prescription to study the effect of edge-mode interaction are plotted up to third order in  $f/J$ , and agree with the exact spectrum in the perturbative, i.e., low  $f/J$ , regime.

### C. Asymmetric $\mathbb{Z}_3$ -parafermion chain

In this subsection we report the same procedure as in Sec. III B while allowing the parafermion chain to deviate from the super-integrable point of the chiral phase by setting  $\phi = \pi/6$  and leaving  $\hat{\phi}$  as a free parameter. In this case, the effective Hamiltonian for the two-site chain up to second order in  $f/J$  is given by

$$H_2^{(2)}(\hat{\phi}) = -\frac{f_1^2 + f_2^2}{J_1} - \frac{f_1 f_2}{J_1} (\bar{\omega} e^{2i\hat{\phi}} \chi_1 \psi_2^\dagger + \omega e^{-2i\hat{\phi}} \psi_2 \chi_1^\dagger) \quad (15)$$

such that the parafermion interaction takes the form

$$H_2^{(2)}(\hat{\phi}) = \begin{pmatrix} 0 & e^{-2i\hat{\phi}} & e^{2i\hat{\phi}} \\ e^{2i\hat{\phi}} & 0 & e^{-2i\hat{\phi}} \\ e^{-2i\hat{\phi}} & e^{2i\hat{\phi}} & 0 \end{pmatrix} \quad (16)$$

up to a global energy shift, which maintains the structure of  $H_2^{(2)}$  in Eq. (12), with an extra phase factor in the interaction term. The eigenvalues of  $H_2^{(2)}(\hat{\phi})$  are given by

$$\begin{aligned} E_0 &= 2 \cos(2\hat{\phi}), & E_1 &= -\cos(2\hat{\phi}) + \sqrt{3} \sin(2\hat{\phi}), \\ E_2 &= -\cos(2\hat{\phi}) - \sqrt{3} \sin(2\hat{\phi}), \end{aligned} \quad (17)$$

where setting  $\hat{\phi} = \frac{\pi}{6}$  recovers the result in Eq. (14). This suggests that by allowing a margin of deviation closer to the ferromagnetic or antiferromagnetic phases of the system,

one can modify the form of the interaction in Eq. (16). We note that while the following will focus on the dynamical gate from the symmetric point, setting the parameter  $\hat{\phi} = \frac{\pi}{4}$ , which still exists in the chiral phase of the chain, gives rise to an interesting eigenspectrum for the purpose of quantum computation.

## IV. NON-CLIFFORD GATE $\mathcal{U}$ FROM PEM INTERACTION

### A. Dynamical gate

The results in Sec. III B show that the interaction between the parafermions edge modes is described by a Hamiltonian which acts nontrivially on the encoded ground space, for which the leading term is shown in Eq. (13). Moreover, one can verify that this interaction (i.e.,  $\omega \chi_1 \psi_L^\dagger + \text{H.c.}$ ) commutes with the parity operator  $\Lambda_1$  defined in Sec. II C and therefore preserves the computational subspace [12]. Hence, bringing the parafermion edge modes closer together allows for a dynamical unitary operation given by the evolution of the interaction Hamiltonian

$$\mathcal{U} \approx e^{-i\beta H_{\text{int}} t}, \quad (18)$$

where  $\beta$  is a constant which depends on the effective coupling between the edge modes, namely up to second order  $\prod_{i=1}^L f_i / \prod_{i=1}^{L-1} J_i$ .

### B. $\mathcal{U}$ in the Clifford hierarchy

The Clifford hierarchy introduced in Sec. II D is useful to categorize the accessible non-Clifford gates using the dynamical gate  $\mathcal{U}$ , and probe geometrically significant gates and eigenstates for fault-tolerant universal quantum computation. In particular, defining gates such as the qudit equivalent of the  $\pi/8$  gate is useful to design magic-state distillation protocols. It was shown in Ref. [38] that a diagonal gate in any level of the Clifford hierarchy for qudits of dimension  $d$  can be written in a diagonal form. The qutrit case is given by

$$U_v = U(v_0, v_1, \dots) = \sum_{j \in \mathbb{Z}_2} \zeta^{v_k} |k\rangle \langle k| \quad (v_k \in \mathbb{Z}_9), \quad (19)$$

where  $\zeta = e^{\frac{2\pi i}{9}}$ ; the indices  $v_k$  are given by  $v_0 = 0 \pmod 9$ ,  $v_1 = 6z' + 2\gamma' + 3\epsilon' \pmod 9$ ,  $v_2 = 6z' + \gamma' + 6\epsilon' \pmod 9$ , and  $z', \gamma', \epsilon' \in \mathbb{Z}_3$ . Following this insight, one can see that the dynamical gate  $\mathcal{U}$  generated by the parafermion interaction on a logical qutrit state can be decomposed as

$$\mathcal{U} = H \mathcal{U}_D H^\dagger, \quad (20)$$

where  $\mathcal{U}$  is the gate in Eq. (18),  $H$  is the qutrit Hadamard operator, and  $\mathcal{U}_D$  the diagonal matrix (up to a global phase) respectively given by the following matrix representations,

$$H = \frac{1}{\sqrt{3}} \begin{pmatrix} 1 & 1 & 1 \\ 1 & \omega & \bar{\omega} \\ 1 & \bar{\omega} & \omega \end{pmatrix}, \quad \mathcal{U}_D \sim \begin{pmatrix} 1 & 0 & 0 \\ 0 & 1 & 0 \\ 0 & 0 & e^{i\theta} \end{pmatrix}, \quad (21)$$

where  $\theta$  is specified by the interaction strength and duration in Eq. (18).

Furthermore, it was shown that analogously to the qubit case, the qutrit  $T$  gate is required to be in  $C_3^{(3)}/C_3^{(2)}$ , i.e., belong in the third level of the Clifford hierarchy but not be a

Clifford gate. For that, one requires that  $TXT^\dagger \in \mathcal{C}^{(2)}$ , where  $X = \sum_{j \in \mathbb{Z}_3} |j+1 \bmod 3\rangle\langle j|$  is the qutrit Pauli- $X$  operator. Since we are interested in which gates we can access with  $\mathcal{U}$ , we similarly verify its action on  $X$  and find that

$$\mathcal{U}_D X \mathcal{U}_D^\dagger = XM(\theta), \quad (22)$$

where  $M(\theta) = \text{diag}\{1, e^{i\theta}, e^{-i\theta}\}$ . In particular,  $M(\frac{2\pi}{3}) = Z$  and  $M(\frac{2\pi}{9}) = T$ , where

$$Z = \sum_{j \in \mathbb{Z}_3} \omega^j |j\rangle\langle j| \quad \text{and} \quad T = \sum_{j \in \mathbb{Z}_3} \zeta^{j^3} |j\rangle\langle j| \quad (23)$$

are matrix representations of the qutrit  $Z$  and  $T$  (analogous to a qubit  $\frac{\pi}{8}$ -phase gate) gates. Hence, for  $\theta = \frac{2\pi}{9}$ ,  $\mathcal{U}_D \in \mathcal{C}^{(4)}$ , i.e., in the fourth level of the Clifford hierarchy.

In general, for a phase  $\theta = \frac{2\pi}{3^m}$ , we can write  $M$  in the following diagonal form [38] where  $p = 3$  is the qudit dimension:

$$M\left(\frac{2\pi}{3^m}\right) = P_m(k) = \sum_{j=0, k \neq j}^p |j\rangle\langle j| + e^{\frac{2\pi i}{3^m}} |k\rangle\langle k|, \quad (24)$$

where  $P_m(k) \in \mathcal{D}_{m,p-1}$ , the set of diagonal qutrit unitaries defined recursively as

$$\mathcal{D}_{m,a} = \langle U_{m,b} \rangle_{b=1}^a \cdot \{e^{i\phi}\} \cdot \mathcal{D}_{m-1,p-1}, \quad (25)$$

$$\text{where } U_{m,b} := \sum_{j \in \mathbb{Z}_p} \exp\left(\frac{2\pi i}{p^m} j^b\right) |j\rangle\langle j|,$$

and  $\{e^{i\phi}\}$  accounts for all global phase shifts. Hence,  $\mathcal{U}_D \in \mathcal{D}_{m,2}$ . Cui *et al.* also showed that for  $m \in \mathbb{N}$  and  $1 \leq a \leq p-1$ ,  $\mathcal{D}_{m,a} = \mathcal{C}_d^{((p-1)(m-1)+a)}$ . According to this result  $\mathcal{D}_{m,2} = \mathcal{C}_d^{(2m)}$ , which signifies that for  $\theta = \frac{2\pi}{3^m}$ , the corresponding  $\mathcal{U}_D$  belong to the  $2m$ th levels of the Clifford hierarchy, i.e.,

$$\mathcal{U}_D \in \mathcal{C}^{(2m)}, \quad (26)$$

so that for  $m \geq 2$ ,  $\mathcal{U}_D$  is a non-Clifford operator. As stated in Eq. (20),  $\mathcal{U}$  is related to  $\mathcal{U}_D$  by a Hadamard operator, which belongs to  $\mathcal{C}^{(2)}$ . We therefore use Theorem 1 in the Appendix to show that for  $\theta = \frac{2\pi}{3^m}$ ,

$$\mathcal{U} \in \mathcal{C}^{(2m)}. \quad (27)$$

Setting  $m = 2$  gives rise to the gate  $\mathcal{U}$  in  $\mathcal{C}^{(4)}$  directly, from which implementing the qutrit  $T$  gate is done with the combination  $T = X^\dagger \mathcal{U}_D X \mathcal{U}_D^\dagger$ .

In order to obtain a set dense in  $SU(d)$ , one requires at least one non-Clifford element in the operational gate set as shown in Ref. [37] for prime  $d$  by combining results from Nebe, Rains, and Sloane [41]. The above illustrates how the parafermion interaction provides such gates, by choosing a parametrization which creates a gate from low levels of the Clifford hierarchy, namely third and fourth. Additionally, we note that the form of the qutrit  $T$  gate arises naturally from the eigenspectrum of the interaction Hamiltonian in Eq. (16) for  $\hat{\phi} = \frac{\pi}{4}$ .

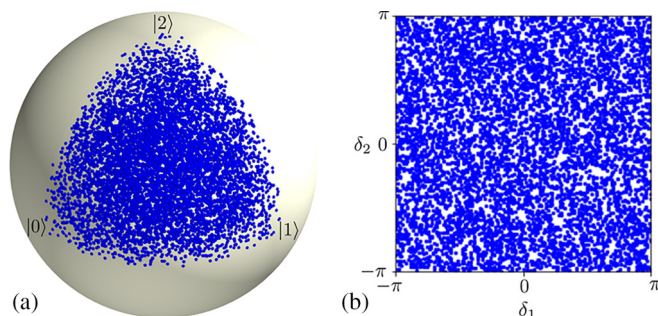


FIG. 5. Magnitude (a) and phase (b) plots for 5000 sampled states computed by creating random words of length 50 using  $\mathcal{U}$  and Clifford operations, and applying them on the initial state  $|\psi\rangle = |0\rangle$ .

### C. Universality with $\mathcal{U}$

In the following, we consider a generic logical qutrit state encoded in a set of parafermions, as described in Sec. II C. In order to study the universality of the parafermion computing scheme that encompasses parafermion zero-mode braiding as well as interaction, we created a series of words  $W := U_1 U_2 \dots U_n$  such that  $U_i$  is chosen randomly from the set  $\{X, S, H, \mathcal{U}\}$  where the first three elements are Clifford operators. In this representation  $S$  takes the form

$$S = \begin{pmatrix} 1 & 0 & 0 \\ 0 & \omega & 0 \\ 0 & 0 & 1 \end{pmatrix}, \quad (28)$$

generalizing the qubit  $\sqrt{Z}$ , and  $H$  is the qutrit Hadamard defined in Eq. (21). The non-Clifford  $\mathcal{U}$  of the set is given by Eq. (18) with  $\theta = 1$  for simplicity. We apply words  $W$  to an initial logical qutrit state  $|\psi_{\text{ini}}\rangle = |0\rangle$ , and write the final states  $|\psi_{\text{fin}}\rangle = W|\psi_{\text{ini}}\rangle$  as  $|\psi_{\text{fin}}\rangle = \alpha|0\rangle + e^{i\delta_1} \beta|1\rangle + e^{i\delta_2} \gamma|2\rangle$ , where  $\alpha, \beta, \gamma \in \mathbb{R}$ . We plot the resulting phases ( $\delta_1, \delta_2$ ) and magnitudes ( $\alpha, \beta, \gamma$ ) from the final states in Figs. 5(a) and 5(c) by sampling 5000 words of length 50 and applying them to  $|\psi_{\text{ini}}\rangle$ . The resulting parameter spaces are densely populated, which indicates the universality of the braiding Clifford operations supplemented with  $\mathcal{U}$ .

### D. Noncontextual qutrit states using $\mathcal{U}$

With the consideration that the set  $\{X, S, H, \mathcal{U}\}$  is dense in  $SU(3)$ , and can be used to generate arbitrary elements in the qutrit-state space using four parafermions, one can characterize such accessible states by their resourcefulness in the context of magic-state distillation (MSD) protocols. Indeed, MSD represents a powerful method to distill reliable quantum states from multiple noisy counterparts, which proves useful in our context since contrary to the Clifford operations, the dynamical gate  $\mathcal{U}$  is nontopological. Moreover, MSD can also be used to obtain useful nonstabilizer states granted one accesses a state in the appropriate distillable region to the former. In Ref. [42], Veitch *et al.* showed that all qutrit states with positive Wigner function are undistillable, and the positive region was charted out in Ref. [18]. In particular, Howard *et al.* argued in Ref. [43] that contextuality supplies the magic for quantum computation, and introduced the following

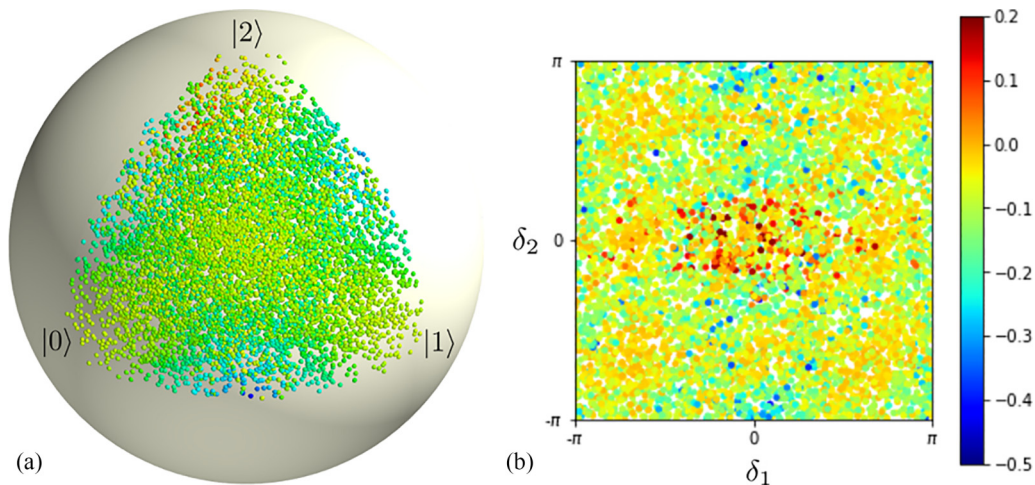


FIG. 6. Magnitude (a) and phase (b) plots of a dense set of 10 000 sampled qutrit states using random words of length 50 composed of the  $\mathcal{U}$  and Clifford operations. The color plot indicates the values of  $\mathcal{M}$ .

contextuality measure

$$\mathcal{M} \equiv \max_{\mathbf{r}} \text{Tr}[A^{\mathbf{r}} \rho] \stackrel{\text{NCHV}}{\leq} 0, \quad (29)$$

where  $\rho$  is an arbitrary qutrit state and the  $A^{\mathbf{r}}$  are projectors onto eigenstates of the qutrit stabilizer operators given by  $A^{x,z} = D^{x,z} A^{0,0} D^{x,z\dagger}$  where  $x, z \in \mathbb{Z}_3$  and  $A^{0,0} = \frac{1}{3} \sum_{x,z} D^{x,z}$  using  $D^{x,z} = \omega^{2xz} X^x Z^z$ , where  $X$  and  $Z$  are the qutrit Pauli operators. The inequality sets the threshold for a noncontextual hidden variable (NCHV) model reproducing such quantum tests. We sampled a large set of qutrit states starting from a random choice of basis states, and plot the negative Wigner states, i.e., violating Eq. (29), indicating their contextuality measure in Fig. 6. In Fig. 6, we see an overlap of points with different  $\mathcal{M}$ . This is clearly due to the fact that the phase and magnitude projections introduced in the figures above do not constitute a direct map of the state space, though they are useful to witness the coverage density of the Hilbert space accessible with our parafermion universal gate set. Indeed, we use this representation as a witness that our gate set provides access to a dense set of negative, and therefore potentially distillable, states. In fact states which considerably violate Eq. (29) can be obtained from short gate combinations [e.g.,  $\mathcal{U}(t_1)H\mathcal{U}(t_2)|0\rangle$  given optimal evolution times  $t_1$  and  $t_2$ ]. We note from Fig. 6 that the majority of the 10 000 sample states created using the full gate set fulfill the condition  $\mathcal{M} < 0$ .

There exists a class of states which maximally violates Eq. (29), namely the “strange” states defined by having one negative Wigner function entry of value  $-1/3$  [44] such as  $|S_a\rangle = \frac{|1\rangle - |2\rangle}{\sqrt{2}}$  [45]. These are the eigenstates of the qutrit Fourier transform, and are located at the midsections between basis states on the magnitude plot as indicated in Fig. 7, with  $\mathcal{M} = -0.5$ . Finding a combination of gates to generate  $|S\rangle$  exactly is a nontrivial problem. However, we show in Fig. 5 that using  $\mathcal{U}$  and Clifford gate combinations one can access states close to the strange states. We indicate in Fig. 7 the points of maximal  $\mathcal{M}$  by labels  $|S_{a,b,c}\rangle$ , and characterize this using the trace distance, i.e.,  $\mathcal{D} = \text{Tr}(\rho, \sigma) = \frac{1}{2} \|\rho - \sigma\|_1$ , where  $\rho$  and  $\sigma$  are the density matrices of the sampled states

and  $|S_{a,b,c}\rangle$ , respectively. In Fig. 7 states with  $\text{Tr}(\rho, \sigma) < 0.2$  are plotted to indicate the regions of interest, and Table I summarizes the trace distances and  $\mathcal{M}$  for the three points closest to the strange states in Fig. 7. We note that both points admit a close to maximal violation of Eq. (29).

Hence, using the Clifford gates supplemented with  $\mathcal{U}$  one can possibly reach states arbitrarily close to the strange states, allowing for large enough gate sequences, and time evolutions in Eq. (18). Recent results in Ref. [46] show how one can distill strange states using an MSD protocol (ternary Golay code [47]) with particularly high threshold. This showcases the advantage of accessing such states.

## V. QUANTUM SIMULATION WITH RYDBERG ATOMS

Rydberg systems offer an attractive potential candidate for quantum simulation, since they possess several advantageous properties [19]. For instance, their strong interactions, long lifetimes, greater than about 50  $\mu\text{s}$  at room temperature, allow high-fidelity state-resolved readout [48,49], high-fidelity entangling operations with  $F > 0.991$  [48], and high-control native multiqubit gates [50]. We also possess various experimental techniques to suppress the error and enhance the fidelity of Rydberg operation suggested in [48,51]. Rydberg systems hold great promise for simulating topologically protected quantum systems. In the light of these facts, Rydberg atoms offer alternative ways to effectively simulate the Hamiltonian as in Eq. (13). In practice, it is preferable to use ground-state hyperfine levels for the qutrit basis states and Rydberg states only for entangling operations.

Here, we propose a setting for the quantum simulation of PEM interaction by engineering the interaction Hamiltonian in the ground-energy three-dimensional subspace with four atomic levels coupled by four classical light fields as shown in Fig. 8(a). In order to use a Rydberg atom to simulate the Hamiltonian as in Eq. (13), we need a three-dimensional Rydberg atom which can be realized by many-photon excitations to 3 different Rydberg states, denoted  $|0\rangle$ ,  $|1\rangle$ , and  $|2\rangle$ . In general, this process is not trivial, since some transitions may be dipole-forbidden due to the selection rule of dipole

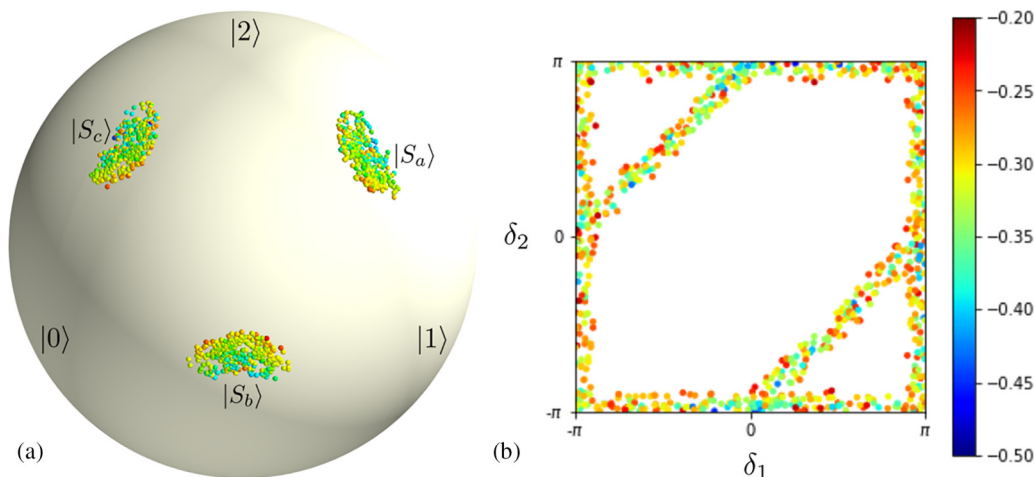


FIG. 7. Magnitude (a) and phase (b) plots of states close to the strange states  $|S_a\rangle$ ,  $|S_b\rangle$ , and  $|S_c\rangle$ , within a trace distance of 0.2. The states were sampled using random words of length 50 composed of the  $\mathcal{U}$  and Clifford operations. The color plot indicates the values of  $\mathcal{M}$ .

interaction. However, this can be overcome by introducing an intermediate state  $|3\rangle$ , which one can later eliminate by performing an adiabatic elimination [see Fig. 8(a) for the setting]. This experimental technique is analogous to the one used in stimulated Raman transitions. In the following procedure, we will first derive the Hamiltonian for a general four-level system and then perform an adiabatic elimination to the intermediate state  $|3\rangle$  that could lead to a desired effective three-level Hamiltonian. We then choose the specific parameters to imitate the Hamiltonian in Eq. (13). All classical light fields are monochromatic microwave laser, described by the overall field

$$\mathbf{E} = \hat{\mathbf{e}}_1 E_1 \cos(\omega_1 t + \phi_1) + \hat{\mathbf{e}}_2 E_2 \cos(\omega_2 t + \phi_2) + \hat{\mathbf{e}}_3 E_3 \cos(\omega_3 t + \phi_3) + \hat{\mathbf{e}}_4 E_4 \cos(\omega_4 t + \phi_4), \quad (30)$$

where  $\hat{\mathbf{e}}_\alpha$  and  $\phi_\alpha$  are a unit polarization vector and relative phase of each field, respectively. The electric fields can then be decomposed into two exponential terms  $\mathbf{E} = \mathbf{E}^{(+)} + \mathbf{E}^{(-)}$ , where  $\mathbf{E}^{(+)} = \sum_{j=1}^4 \frac{1}{2} \hat{\mathbf{e}}_j E_j e^{-i(\omega_j t + \phi_j)}$  is the positive-rotating component and  $\mathbf{E}^{(-)} = \sum_{j=1}^4 \frac{1}{2} \hat{\mathbf{e}}_j E_j e^{i(\omega_j t + \phi_j)}$  is the negative-rotating. Additionally, we assume that the wavelength of the field is much longer than the size of the atom. Hence, the spatial dependence of the field can be ignored over the size of the atom as per the dipole approximation.

Since the dipole operator  $\mathbf{d} = -e\mathbf{r}_e$  is an odd-parity operator, its diagonal elements vanish, and the (real) dipole matrix

elements of each coupling pair are given by

$$\mathbf{d} = \langle 0|\mathbf{d}|1\rangle(\sigma_1 + \sigma_1^\dagger) + \langle 0|\mathbf{d}|2\rangle(\sigma_2 + \sigma_2^\dagger) + \langle 2|\mathbf{d}|3\rangle(\sigma_3 + \sigma_3^\dagger) + \langle 0|\mathbf{d}|3\rangle(\sigma_4 + \sigma_4^\dagger), \quad (31)$$

where  $\sigma_1 = |0\rangle\langle 1|$ ,  $\sigma_2 = |1\rangle\langle 2|$ ,  $\sigma_3 = |2\rangle\langle 3|$ , and  $\sigma_4 = |0\rangle\langle 3|$ . Under free atomic evolution, the expectation values of  $\sigma_{1,2,3,4}$  have unperturbed time-dependence terms of  $e^{-i\omega_{01}t}$ ,  $e^{-i(\omega_{02}-\omega_{01})t}$ ,  $e^{-i(\omega_{03}-\omega_{02})t}$ ,  $e^{-i\omega_{03}t}$  which are all positive-rotating. These terms can be considered as  $\mathbf{d}^{(+)}$ . Similarly, the expectation values of  $\sigma_{1,2,3,4}^\dagger$  have unperturbed time dependence of opposite sign, which therefore can be considered as  $\mathbf{d}^{(-)}$ , such that the dipole operator can be decomposed as  $\mathbf{d} = \mathbf{d}^{(+)} + \mathbf{d}^{(-)}$ . The interaction Hamiltonian caused by dipole interaction is given by  $\hat{H}_{\text{int}} = -\mathbf{d} \cdot \mathbf{E}$ . After applying the rotating-wave approximation which focuses on slow dynamics rather than fast, thereby ignoring interaction terms  $\mathbf{d}^{(+)} \cdot \mathbf{E}^{(+)}$  and  $\mathbf{d}^{(-)} \cdot \mathbf{E}^{(-)}$ , the interaction Hamiltonian

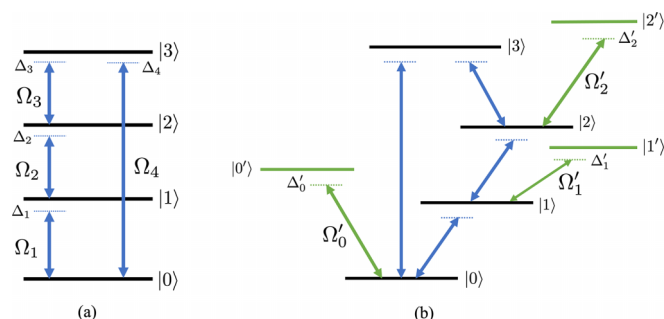


FIG. 8. (a) The four-level atomic system coupled by four monochromatic classical microwave fields, where we indicate the respective Rabi frequencies and detunings between our levels by  $\Omega_i$  and  $\Delta_i$  for  $i \in \{1, 2, 3, 4\}$ . (b) The additional states  $|0'\rangle$ ,  $|1'\rangle$ , and  $|2'\rangle$  coupled to states  $|0\rangle$ ,  $|1\rangle$ , and  $|2\rangle$  with Rabi frequencies  $\Omega'_0$ ,  $\Omega'_1$ ,  $\Omega'_2$  and detunings  $\Delta'_0$ ,  $\Delta'_1$ ,  $\Delta'_2$ , respectively. These additional couplings are to induce the light shifts that could compensate out the diagonal terms.

TABLE I. Trace distances  $\mathcal{D}$  and noncontextuality measure  $\mathcal{M}$  of the three sampled states in Fig. 7 closest to  $|S_a\rangle$ ,  $|S_b\rangle$ , and  $|S_c\rangle$ .

	$ S_a\rangle$	$ S_b\rangle$	$ S_c\rangle$
$\mathcal{D}$	0.059	0.057	0.035
$\mathcal{M}$	-0.436	-0.422	-0.469



becomes

$$\begin{aligned}\hat{H}_{\text{int}} &= -(\mathbf{d}^{(+)} \cdot \mathbf{E}^{(-)} + \mathbf{d}^{(-)} \cdot \mathbf{E}^{(+)}) \\ &= \frac{\Omega_1}{2}(\sigma_1 e^{i(\omega_1 t + \phi_1)} + \sigma_1^\dagger e^{-i(\omega_1 t + \phi_1)}) \\ &\quad + \frac{\Omega_2}{2}(\sigma_2 e^{i(\omega_2 t + \phi_2)} + \sigma_2^\dagger e^{-i(\omega_2 t + \phi_2)}) \\ &\quad + \frac{\Omega_3}{2}(\sigma_3 e^{i(\omega_3 t + \phi_3)} + \sigma_3^\dagger e^{-i(\omega_3 t + \phi_3)}) \\ &\quad + \frac{\Omega_4}{2}(\sigma_4 e^{i(\omega_4 t + \phi_4)} + \sigma_4^\dagger e^{-i(\omega_4 t + \phi_4)}),\end{aligned}\quad (32)$$

where the Rabi frequencies for each coupling pair are  $\Omega_1 = -\langle 0|\hat{\epsilon}_1 \cdot \mathbf{d}|1\rangle E_1$ ,  $\Omega_2 = -\langle 1|\hat{\epsilon}_2 \cdot \mathbf{d}|2\rangle E_2$ ,  $\Omega_3 = -\langle 0|\hat{\epsilon}_3 \cdot \mathbf{d}|3\rangle E_3$ , and  $\Omega_4 = -\langle 0|\hat{\epsilon}_4 \cdot \mathbf{d}|3\rangle E_4$ . The free atomic

Hamiltonian is defined as

$$\hat{H}_A = \omega_{01}|1\rangle\langle 1| + \omega_{02}|2\rangle\langle 2| + \omega_{03}|3\rangle\langle 3|, \quad (33)$$

where  $|0\rangle$  denotes the zero-energy ground state. The evolution of the system is calculated by solving the Schrödinger equation  $i\partial_t|\tilde{\psi}\rangle = (\hat{H}_A + \hat{H}_{\text{int}})|\tilde{\psi}\rangle$ . The state  $|\tilde{\psi}\rangle$  is defined as the quantum state in the rotating frame. In this frame, we assume that the state  $|3\rangle$  maintains the same velocity of its dynamics in the original frame, while other states are sped up with different velocities such that  $|\tilde{\psi}\rangle = \tilde{c}_0|0\rangle + \tilde{c}_1|1\rangle + \tilde{c}_2|2\rangle + c_3|3\rangle$  where  $\tilde{c}_0 = e^{-i(\omega_1 + \omega_2 + \omega_3)t} c_0$ ,  $\tilde{c}_1 = e^{-i(\omega_2 + \omega_3)t} c_1$ , and  $\tilde{c}_2 = e^{-i\omega_3 t} c_2$ . The multiplied exponential factors are inserted to fasten the dynamics of states  $|0\rangle$ ,  $|1\rangle$ , and  $|2\rangle$ . It can be shown that the resulting Hamiltonian under which the state  $|\tilde{\psi}\rangle$  evolves is explicitly time-independent when the condition  $\Delta_4 = \Delta_1 + \Delta_2 + \Delta_3$  is satisfied, also known as the four-photon resonance condition. The time-independent Schrödinger equation is given by

$$i\partial_t \begin{pmatrix} \tilde{c}_0 \\ \tilde{c}_1 \\ \tilde{c}_2 \\ c_3 \end{pmatrix} = \begin{pmatrix} -(\Delta_1 + \Delta_2 + \Delta_3) & \frac{\Omega_1}{2} e^{i\phi_1} & 0 & \frac{\Omega_4}{2} e^{i\phi_4} \\ \frac{\Omega_1}{2} e^{-i\phi_1} & -(\Delta_2 + \Delta_3) & \frac{\Omega_2}{2} e^{i\phi_2} & 0 \\ 0 & \frac{\Omega_2}{2} e^{-i\phi_2} & -\Delta_3 & \frac{\Omega_3}{2} e^{i\phi_3} \\ \frac{\Omega_4}{2} e^{-i\phi_4} & 0 & \frac{\Omega_3}{2} e^{-i\phi_3} & 0 \end{pmatrix} \begin{pmatrix} \tilde{c}_0 \\ \tilde{c}_1 \\ \tilde{c}_2 \\ c_3 \end{pmatrix}, \quad (34)$$

where for convenience the energy reference is adjusted such that the state  $|3\rangle$  is the zero-energy level.

Since the ground subspace of the parafermion chain is three-dimensional, we will perform *an adiabatic elimination* to the system's equations of motion in Eq. (34), which yields the effective three-level Hamiltonian that can simulate the three-dimensional subspace. First, we multiply the overall phase factor  $e^{i\Delta t}$  to the system's four-state vector to shift all the energy level by  $\Delta$ . This has no physical impact on quantum state since their relative phases do not change. However, to satisfy the condition of an adiabatic elimination, the  $\Delta$ , which is the fast-oscillation term of  $c_3$  from the Schrödinger equation, needs to be much larger compared to other oscillation terms for  $\tilde{c}_0$ ,  $\tilde{c}_1$ , and  $\tilde{c}_2$ , i.e.,  $|\Delta| \gg |\Delta - \Delta_3|$ ,  $|\Delta - (\Delta_2 + \Delta_3)|$ ,  $|\Delta - (\Delta_1 + \Delta_2 + \Delta_3)|$ . The last three terms here are respectively the oscillation terms for  $\tilde{c}_2$ ,  $\tilde{c}_1$ , and  $\tilde{c}_0$  after multiplying  $e^{i\Delta t}$ . To make sure that the state  $|3\rangle$  is never populated, the conditions  $\Delta_3 \gg \Omega_3$  and  $\Delta_4 \gg \Omega_4$

are required. Besides, the condition  $|\Delta_{3,4}| \gg \Gamma$ , where  $\Gamma$  is natural decay rate of the state  $|3\rangle$ , is also needed to make sure that the spontaneous emission can be negligible. For convenience, we can set  $\Delta = \Delta_3 = \Delta_4$ , and the overall constraints on  $\Delta$  by the above conditions due to an adiabatic elimination are (1)  $|\Delta| \gg |\Delta_1| + |\Delta_2|$ , (2)  $|\Delta| \gg |\Omega_{3,4}|$ , (3)  $|\Delta| \gg \Gamma$ . Considering the equation of motion for  $c_3$ , when  $\Delta$  is satisfied for all the above conditions, it is obvious that  $c_3$  carries the fast oscillation at frequencies of order  $|\Delta| \gg \Gamma$  so that  $c_3$  is damped by coupling to the vacuum on timescales of  $1/\Gamma$ . Here, we only consider the motions on timescales slow compared to  $1/\Gamma$ , i.e.,  $\tilde{c}_2$ ,  $\tilde{c}_1$ , and  $\tilde{c}_0$ , and thus can make the approximation that  $c_3$  damps to equilibrium instantaneously, i.e.,  $\partial_t c_3 = 0$ . Therefore, we can obtain the substitution for  $c_3$  by  $\tilde{c}_0$ ,  $\tilde{c}_1$ ,  $\tilde{c}_2$  from the last equation of Eq. (34) such that  $c_3 = -(\frac{\Omega_4}{2\Delta} e^{-i\phi_4} \tilde{c}_0 + \frac{\Omega_3}{2\Delta} e^{-i\phi_3} \tilde{c}_2)$ . Substituting this into the equation for  $\tilde{c}_0$ ,  $\tilde{c}_1$ ,  $\tilde{c}_2$  in Eq. (34), we finally obtain the effective three-level Hamiltonian in which the state  $|3\rangle$  is eliminated,

$$i\partial_t \begin{pmatrix} \tilde{c}_0 \\ \tilde{c}_1 \\ \tilde{c}_2 \end{pmatrix} = \begin{pmatrix} -(\Delta_1 + \Delta_2 + \Delta_3 + \frac{\Omega_4^2}{4\Delta}) & \frac{\Omega_1}{2} e^{i\phi_1} & \frac{-\Omega_4\Omega_3}{4\Delta} e^{i(\phi_4 - \phi_3)} \\ \frac{\Omega_1}{2} e^{-i\phi_1} & -(\Delta_2 + \Delta_3) & \frac{\Omega_2}{2} e^{i\phi_2} \\ \frac{-\Omega_4\Omega_3}{4\Delta} e^{-i(\phi_4 - \phi_3)} & \frac{\Omega_2}{2} e^{-i\phi_2} & -(\Delta_3 + \frac{\Omega_3^2}{4\Delta}) \end{pmatrix} \begin{pmatrix} \tilde{c}_0 \\ \tilde{c}_1 \\ \tilde{c}_2 \end{pmatrix}. \quad (35)$$

Since the states  $|0\rangle$  and  $|2\rangle$  initially interact directly with the state  $|3\rangle$ , the adiabatic elimination of the state  $|3\rangle$  gives rise to an effective Rabi coupling between the states  $|0\rangle$  and  $|2\rangle$ , which is  $\Omega_R = \frac{-\Omega_4\Omega_3}{2\Delta} e^{i(\phi_4 - \phi_3)}$ . Additionally, the energy

terms are also shifted due to AC Stark shifts, amounting to  $\Omega_4^2/(4\Delta)$  and  $\Omega_3^2/(4\Delta)$  for the states  $|0\rangle$  and  $|2\rangle$ , respectively. In order to recover the parafermion interaction Hamiltonian given in Eq. (13), we first need all the diagonal terms to

be zero. This can be realized by coupling the states  $|0\rangle$ ,  $|1\rangle$  and  $|2\rangle$  to complemented states  $|0'\rangle$ ,  $|1'\rangle$ , and  $|2'\rangle$ , respectively, as shown in Fig. 8(b). This is to allow the additional light shifts, i.e.,  $\Omega_0^2/4\Delta_0'$ ,  $\Omega_1^2/4\Delta_1'$ , and  $\Omega_2^2/4\Delta_2'$ , for each diagonal term to be canceled. Experimentally, one can choose the complemented states and parameters such that the diagonal terms disappear. Additionally, the nondiagonal terms can also be set to simulate the Hamiltonian as in Eq. (13) by choosing the states and parameters such that  $|\Omega_1| = |\frac{\Omega_3\Omega_4}{2\Delta}| = |\Omega_2| = g$ , and relative phases of the laser fields following  $\phi_1 = \phi_2 = -(\phi_4 - \phi_3) = \frac{2\pi}{3}$ , where  $g$  is a controllable factor depending on laser detuning.

By fixing the external field parameters according to these identities, we can implement the braiding of parafermions, by realizing a Berry phase evolution on states  $|2\rangle$  and  $|3\rangle$ . This entails turning on solely the interaction between the latter states, and allowing for an adiabatic evolution in order for a geometric phase to accumulate, as described in Ref. [52], where it was shown that the adiabatic evolution of a two-level model in the presence of an external classical electric field yields the Berry phase,

$$\gamma_l = \frac{l}{2} \oint_0^T dt \frac{|D(t)|^2}{F_l(t)} \dot{\phi}_3(t), \quad (36)$$

where  $l$  indicates the instantaneous eigenstates of the model,  $D(t) = \langle 2|\mathbf{d}|3\rangle \cdot \hat{\epsilon}_3 E_3(t)$ ,  $F_l(t) = (\frac{\omega_{23}}{2})^2 + |D(t)|^2 - l \cdot (\frac{\omega_{23}}{2}) \sqrt{(\frac{\omega_{23}}{2})^2 + |D(t)|^2}$ , and  $\phi_3(t)$  is the time-dependent relative phase of the coupling laser between states  $|2\rangle$  and  $|3\rangle$ . While dynamical phases arise in this procedure, leading to unwanted dephasing in the time evolution, these can be closely monitored and compensated for. Indeed, to cancel out the dynamical phase accumulated in the adiabatic evolution, the other coupling channels are turned on, as shown in Fig. 8. This allows us to apply adiabatic elimination to state  $|3\rangle$ , which yields the additional AC Stark shift to state  $|2\rangle$  that destructively compensates for the unwanted dephasing, leaving only the geometric phase. This corresponds to the Berry phase required to simulate the braiding of parafermions as derived in Eq. (A6) in Ref. [12].

## VI. DISCUSSION

Motivated by the use of direct short-range interaction between Majorana quasiparticles to achieve the  $\frac{\pi}{8}$ -phase gate on a topologically encoded qubit [17], we investigated a similar prescription in the case of  $\mathbb{Z}_3$  parafermions. We studied the interaction between the edge modes of a parafermion chain using exact perturbation for low orders, in order to find its effect on the degenerate ground space of the system, which is used to encode one qutrit. We find that allowing the edge modes a degree of delocalization facilitates the generation of a nontopological dynamical gate. In particular, the structure of this gate can directly be exploited to realize interesting non-Clifford operations such as the qutrit equivalent of the (qubit)  $\frac{\pi}{8}$ -phase gate (provided access to extra Clifford operations), as well as unitaries in higher levels of the Clifford hierarchy. This is a crucial complement to the topological operations since the addition of any non-Clifford gate to the Clifford group generates a set of unitaries that is dense in  $SU(d)$  [37]. We

illustrated this universality by sampling states obtained with Clifford operations (as provided by braiding parafermions [12]), complemented with the dynamical non-Clifford gate  $\mathcal{U}$ , visualized using two parameter spaces which we defined to characterize qutrit states. While such representations served their purpose within our study, we refer the reader to the recent Ref. [53] by Eltschka *et al.* for a three-dimensional model of the qutrit-state space that captures its prominent and essential geometric features. We additionally adopted recent results on the universality of one-qudit gates [54] in order to test our gate set supplemented with the nontopological  $\mathcal{U}$  with success, which was completed as a sanity check and left outside the scope of our presented results.

The non-Clifford gate accessible through PEM interaction is not topologically protected. However, fault tolerance can be reinstated using stabilizer operations in a magic-state distillation protocol [17,18,37]. Contextuality represents a critical resource for MSD and can be characterized by a state-independent measure  $\mathcal{M}$  [43]. Using this result we showed that our gate set provides noncontextual states under stabilizer measurements, which can be exploited in appropriate distillation routines. While we studied the  $\mathbb{Z}_3$  case for convenience, one could generalize the above analysis to  $\mathbb{Z}_d$  parafermion edge-mode interaction, particularly for prime odd  $d$  as the emergent gates are of interest in the context of quantum information processing.

Finally, we showed how the two-parafermion (edge-mode) interaction and braiding can be simulated using a four-level Rydberg system, offering an experimental setting for probing simulated topological qudits. Alternatively, it has been suggested to use ultracold molecules to realize qudits with different four vibrational levels as shown in [55] which benefits from its longer coherence time [56]. However, the strength of dipole-dipole interactions between molecules remains less significant than in the case of Rydberg atoms, making them more favorable to implement a qutrit. Finally, it is worth mentioning that quantum simulations with qutrits might yield a novel tool for studying quantum many-body physics such as quantum phase transitions and out-of-equilibrium phenomena. It is of interest that the Hamiltonian of many qutrit systems with dipole-dipole interactions can show quantum phase transitions or topological effects which might yield exotic results in condensed matter physics. As an example, in recent work from Blok *et al.* [57] quantum information scrambling was witnessed on a superconducting processor which can provide insight into quantum chaos and black hole dynamics.

## ACKNOWLEDGMENTS

A.B. acknowledges funding from the EPSRC Centre for Doctoral Training in Delivering Quantum Technologies at UCL, Grant No. EP/S021582/1L. D.E.B. was supported by the Quanterra project Quantum Codes Design and Architecture, EPSRC Grant No. EP/R043647/1, and J.K.P. from EPSRC Grant No. EP/R020612/1. T.A. and C.S.A. are supported by EPSRC Grants No. EP/V030280/1, No. EP/V047302/1, No. EP/S015973/1, No. EP/R035482/1, No. EP/R002061/1, and No. EP/P012000/1.

### APPENDIX: THE GATE $U$ IN THE CLIFFORD HIERARCHY

*Theorem 1.* Let  $U = HVH^\dagger$  where  $H \in \mathcal{C}^{(2)}$ ,  $V \in \mathcal{C}^{(n)}$ , and  $\mathcal{C}^{(k)}$  is  $k$ th level of the Clifford hierarchy,  $U \in \mathcal{C}^{(n)}$ .

In order to prove this succinctly we define Lemma 1 below which follows from Eq. (8) along with the observation that  $H^3 = H^\dagger$ .

*Lemma 1.* Let  $U \in \mathcal{C}^{(k)}$  and  $P \in \mathcal{C}^{(1)}$ ,

$$(HUH^\dagger)P(HU^\dagger H^\dagger) = H\tilde{U}H^\dagger, \quad (\text{A1})$$

where  $\tilde{U} \in \mathcal{C}^{(k-1)}$ .

*Proof of Theorem 1.* Let  $V \in \mathcal{C}^{(n)}$  and  $P$  be an arbitrary Pauli operator such that  $VPV^\dagger \in \mathcal{C}^{(n-1)}$ . We define the unitary operator  $U = HVH^\dagger$ . Using Lemma 1 the following ensues,

$$UPU^\dagger \sim H\beta_{n-1}H^\dagger, \quad (\text{A2})$$

where  $\beta_i$  is a unitary operator in the  $i$ th level of the Clifford hierarchy, i.e.,  $\beta_i \in \mathcal{C}^{(i)}$ . The case for  $n = 2$  is straightforward as  $VPV^\dagger \in \mathcal{C}^{(1)}$ , from which we obtain

$$(HVH^\dagger)P(HV^\dagger H^\dagger) \in \mathcal{C}^{(1)}. \quad (\text{A3})$$

For general  $n \geq 3$ , one can start from Eq. (A2) and again act on an arbitrary Pauli operator with  $H\beta_{n-1}H^\dagger$  to find that

$$(H\beta_{n-1}H^\dagger)P(H\beta_{n-1}^\dagger H^\dagger) \sim H\beta_{n-2}H^\dagger, \quad (\text{A4})$$

where  $P \in \mathcal{C}^{(1)}$ . One can iterate this procedure  $m$  times such that for  $m = 0$ ,

$$(H\beta_n H^\dagger)P(H\beta_n^\dagger H^\dagger) \sim H\beta_{n-1}H^\dagger, \quad (\text{A5})$$

and subsequently for general  $m$ ,

$$(H\beta_{n-m}H^\dagger)P(H\beta_{n-m}^\dagger H^\dagger) \sim H\beta_{n-m-1}H^\dagger. \quad (\text{A6})$$

Finally, when  $m = n - 3$ ,

$$(H\beta_3 H^\dagger)P(H\beta_3^\dagger H^\dagger) \sim H\beta_2 H^\dagger, \quad (\text{A7})$$

where one identifies  $H\beta_2 H^\dagger \in \mathcal{C}^{(2)}$ . Using Eq. (A5) recursively, it is then straightforward to show that  $H\beta_n H^\dagger \in \mathcal{C}^{(n)}$ , and therefore  $U \in \mathcal{C}^{(n)}$ .

- 
- [1] A. Yu. Kitaev, Fault-tolerant quantum computation by anyons, *Ann. Phys.* **303**, 2 (2003).
- [2] E. Knill, Quantum computing with realistically noisy devices, *Nature (London)* **434**, 39 (2005).
- [3] P. W. Shor, Fault-tolerant quantum computation, in *Proceedings of 37th Conference on Foundations of Computer Science (IEEE, 1996)*, pp. 56–65.
- [4] R. W. Ogburn and J. Preskill, Topological quantum computation, in *Quantum Computing and Quantum Communications*, edited by Colin P. Williams (Springer, Berlin, 1999), pp. 341–356.
- [5] M. H. Freedman, A. Kitaev, M. J. Larsen, and Z. Wang, Topological quantum computation, *Bull. Am. Math. Soc.* **40**, 31 (2003).
- [6] A. Yu. Kitaev, Unpaired Majorana fermions in quantum wires, *Phys. Usp.* **44**, 131 (2001).
- [7] A. Kitaev, Anyons in an exactly solved model and beyond, *Ann. Phys.* **321**, 2 (2006).
- [8] G. Moore and N. Read, Nonabelions in the fractional quantum hall effect, *Nucl. Phys. B* **360**, 362 (1991).
- [9] P. Fendley, Parafermionic edge zero modes in  $\mathbb{Z}_n$ -invariant spin chains, *J. Stat. Mech.: Theory Exp.* (2012) P11020.
- [10] S. Das Sarma, M. Freedman, and C. Nayak, Majorana zero modes and topological quantum computation, *npj Quantum Inf.* **1**, 15001 (2015).
- [11] D. Clarke, J. Alicea, and K. Shtengel, Exotic non-Abelian anyons from conventional fractional quantum Hall states, *Nat. Commun.* **4**, 1348 (2013).
- [12] A. Hutter and D. Loss, Quantum computing with parafermions, *Phys. Rev. B* **93**, 125105 (2016).
- [13] N. H. Lindner, E. Berg, G. Refael, and A. Stern, Fractionalizing Majorana Fermions: Non-Abelian Statistics on the Edges of Abelian Quantum Hall States, *Phys. Rev. X* **2**, 041002 (2012).
- [14] D. Gottesman, The Heisenberg representation of quantum computers, *arXiv:quant-ph/9807006*.
- [15] D. Gottesman, Theory of fault-tolerant quantum computation, *Phys. Rev. A* **57**, 127 (1998).
- [16] S. Bravyi, Universal quantum computation with the  $\nu = 5/2$  fractional quantum Hall state, *Phys. Rev. A* **73**, 042313 (2006).
- [17] S. Bravyi and A. Kitaev, Universal quantum computation with ideal Clifford gates and noisy ancillas, *Phys. Rev. A* **71**, 022316 (2005).
- [18] H. Anwar, E. T. Campbell, and D. E. Browne, Qutrit magic state distillation, *New J. Phys.* **14**, 063006 (2012).
- [19] M. Morgado and S. Whitlock, Quantum simulation and computing with Rydberg-interacting qubits, *AVS Quan. Sci.* **3**, 023501 (2021).
- [20] C. S. Adams, J. D. Pritchard, and J. P. Shaffer, Rydberg atom quantum technologies, *J. Phys. B* **53**, 012002 (2019).
- [21] A. Browaeys and T. Lahaye, Many-body physics with individually controlled Rydberg atoms, *Nat. Phys.* **16**, 132 (2020).
- [22] H. Weimer, M. Müller, I. Lesanovsky, P. Zoller, and H. P. Büchler, A Rydberg quantum simulator, *Nat. Phys.* **6**, 382 (2010).
- [23] S. Ebadi, T. T. Wang, H. Levine, A. Keesling, G. Semeghini, A. Omran, D. Bluvstein, R. Samajdar, H. Pichler, W. W. Ho *et al.*, Quantum phases of matter on a 256-atom programmable quantum simulator, *Nature (London)* **595**, 227 (2021).
- [24] R. Verresen, M. D. Lukin, and A. Vishwanath, Prediction of Toric Code Topological Order from Rydberg Blockade, *Phys. Rev. X* **11**, 031005 (2021).
- [25] V. Lienhard, P. Scholl, S. Weber, D. Barredo, S. de Léséleuc, R. Bai, N. Lang, M. Fleischhauer, H. P. Büchler, T. Lahaye, and A. Browaeys, Realization of a Density-Dependent Peierls Phase in a Synthetic, Spin-Orbit Coupled Rydberg System, *Phys. Rev. X* **10**, 021031 (2020).
- [26] D. Barredo, H. Labuhn, S. Ravets, T. Lahaye, A. Browaeys, and C. S. Adams, Coherent Excitation Transfer in a Spin Chain of Three Rydberg Atoms, *Phys. Rev. Lett.* **114**, 113002 (2015).

- [27] N. L. R. Spong, Y. Jiao, O. D. W. Hughes, K. J. Weatherill, I. Lesanovsky, and C. S. Adams, Collectively Encoded Rydberg Qubit, *Phys. Rev. Lett.* **127**, 063604 (2021).
- [28] P. Gokhale, J. M. Baker, C. Duckering, N. C. Brown, K. R. Brown, and F. T. Chong, Asymptotic improvements to quantum circuits via qutrits, in *Proceedings of the 46th International Symposium on Computer Architecture* (ACM, 2019).
- [29] Y. Zhuang, H. J. Changlani, N. M. Tubman, and T. L. Hughes, Phase diagram of the  $\mathbb{Z}_3$  parafermionic chain with chiral interactions, *Phys. Rev. B* **92**, 035154 (2015).
- [30] I. Mahyaeh, J. Wouters, and D. Schuricht, Phase diagram of the  $\mathbb{Z}_3$ -Fock parafermion chain with pair hopping, *SciPost Phys. Core* **3**, 011 (2020).
- [31] N. Moran, D. Pellegrino, J. K. Slingerland, and G. Kells, Parafermionic clock models and quantum resonance, *Phys. Rev. B* **95**, 235127 (2017).
- [32] M. Jimbo, Introduction to the Yang-Baxter equation, *Int. J. Mod. Phys. A* **4**, 3759 (1989).
- [33] J. M. Farinholt, An ideal characterization of the Clifford operators, *J. Phys. A: Math. Theor.* **47**, 305303 (2014).
- [34] D. Gottesman and I. L. Chuang, Demonstrating the viability of universal quantum computation using teleportation and single-qubit operations, *Nature (London)* **402**, 390 (1999).
- [35] P. O. Boykin, T. Mor, M. Pulver, V. Roychowdhury, and F. Vatan, A new universal and fault-tolerant quantum basis, *Inf. Process. Lett.* **75**, 101 (2000).
- [36] M. Howard and J. Vala, Qudit versions of the qubit  $\pi/8$  gate, *Phys. Rev. A* **86**, 022316 (2012).
- [37] E. T. Campbell, H. Anwar, and D. E. Browne, Magic-State Distillation in All Prime Dimensions Using Quantum Reed-Muller Codes, *Phys. Rev. X* **2**, 041021 (2012).
- [38] S. X. Cui, D. Gottesman, and A. Krishna, Diagonal gates in the Clifford hierarchy, *Phys. Rev. A* **95**, 012329 (2017).
- [39] D. S. Fisher, Critical behavior of random transverse-field Ising spin chains, *Phys. Rev. B* **51**, 6411 (1995).
- [40] V. Shivamoggi, Majorana fermions and Dirac edge states in topological phases, Ph.D. thesis, University of California, Berkeley, 2011.
- [41] G. Nebe, E. M. Rains, and N. J. A. Sloane, *Self-Dual Codes and Invariant Theory* (Springer, 2010).
- [42] V. Veitch, C. Ferrie, D. Gross, and J. Emerson, Negative quasiprobability as a resource for quantum computation, *New J. Phys.* **14**, 113011 (2012).
- [43] M. Howard, J. Wallman, V. Veitch, and J. Emerson, Contextuality supplies the “magic” for quantum computation, *Nature (London)* **510**, 351 (2014).
- [44] V. Veitch, S. A. Hamed Mousavian, D. Gottesman, and J. Emerson, The resource theory of stabilizer quantum computation, *New J. Phys.* **16**, 013009 (2014).
- [45] A. Jain and S. Prakash, Qutrit and ququint magic states, *Phys. Rev. A* **102**, 042409 (2020).
- [46] S. Prakash, Magic state distillation with the ternary Golay code, *Proc. R. Soc. A* **476**, 20200187 (2020).
- [47] V. Pless, On the uniqueness of the Golay codes, *J. Comb. Theory* **5**, 215 (1968).
- [48] I. S. Madjarov, J. P. Covey, A. L. Shaw, J. Choi, A. Kale, A. Cooper, H. Pichler, V. Schkolnik, J. R. Williams, and M. Endres, High-fidelity entanglement and detection of alkaline-earth Rydberg atoms, *Nat. Phys.* **16**, 857 (2020).
- [49] J. P. Covey, I. S. Madjarov, A. Cooper, and M. Endres, 2000-Times Repeated Imaging of Strontium Atoms in Clock-Magic Tweezer Arrays, *Phys. Rev. Lett.* **122**, 173201 (2019).
- [50] H. Levine, A. Keesling, G. Semeghini, A. Omran, T. T. Wang, S. Ebadi, H. Bernien, M. Greiner, V. Vuletić, H. Pichler *et al.*, Parallel Implementation of High-Fidelity Multiqubit Gates with Neutral Atoms, *Phys. Rev. Lett.* **123**, 170503 (2019).
- [51] H. Levine, A. Keesling, A. Omran, H. Bernien, S. Schwartz, A. S. Zibrov, M. Endres, M. Greiner, V. Vuletić, and M. D. Lukin, High-Fidelity Control and Entanglement of Rydberg-Atom Qubits, *Phys. Rev. Lett.* **121**, 123603 (2018).
- [52] A. C. Aguiar Pinto, M. Moutinho, and M. T. Thomaz, Berry’s phase in the two-level model, *Braz. J. Phys.* **39**, 326 (2009).
- [53] C. Eltschka, M. Huber, S. Morelli, and J. Siewert, The shape of higher-dimensional state space: Bloch-ball analog for a qutrit, *Quantum* **5**, 485 (2021).
- [54] A. Sawicki and K. Karnas, Universality of single-qudit gates, *Ann. Henri Poincaré* **18**, 3515 (2017).
- [55] R. Sawant, J. A. Blackmore, P. D. Gregory, J. Mur-Petit, D. Jaksch, J. Aldegunde, J. M. Hutson, M. R. Tarbutt, and S. L. Cornish, Ultracold polar molecules as qudits, *New J. Phys.* **22**, 013027 (2020).
- [56] P. D. Gregory, J. A. Blackmore, S. L. Bromley, J. M. Hutson, and S. L. Cornish, Robust storage qubits in ultracold polar molecules, *Nat. Phys.* **17**, 1149 (2021).
- [57] M. S. Blok, V. V. Ramasesh, T. Schuster, K. O’Brien, J. M. Kreikebaum, D. Dahlen, A. Morvan, B. Yoshida, N. Y. Yao, and I. Siddiqi, Quantum Information Scrambling on a Superconducting Qutrit Processor, *Phys. Rev. X* **11**, 021010 (2021).